

Cite this: *Dalton Trans.*, 2020, **49**, 1249

Stereochemistry of coordination polyhedra vs. single ion magnetism in penta- and hexacoordinated Co(II) complexes with tridentate rigid ligands†

Barbora Brachňáková,^a Simona Matejová,^a Ján Moncol,^a Radovan Herchel,^b Ján Pavlík,^a Eufemio Moreno-Pineda,^c Mario Ruben^{c,d} and Ivan Šalitroš^{a,b,e}

A tridentate ligand **L** (2,6-bis(1-(3,5-di-*tert*-butylbenzyl)-1*H*-benzimidazol-2-yl)pyridine) was synthesized and used for the preparation of three pentacoordinated Co(II) complexes of formula [Co(L)X₂] (where X = NCS⁻ for **1**, X = Cl⁻ for **2** and X = Br⁻ for **3**) and one ionic compound **4** ([Co(L)₂]Br₂·2CH₃OH·H₂O) containing a hexacoordinated Co(II) centre. Static magnetic data were analysed with respect to the spin (**1–3**) or the Griffith–Figgis (**4**) Hamiltonian. *Ab initio* calculations enable us to identify the positive axial magnetic anisotropy parameter *D* accompanied by a significant degree of rhombicity in the reported complexes. Also, magneto-structural correlation was outlined for this class of compounds. Moreover, all four compounds exhibit slow relaxation of magnetisation at an applied static magnetic field with either both low- and high-frequency relaxation channels (**3**) or a single high-frequency relaxation process (**1**, **2** and **4**). The interplay between the stereochemistry of coordination polyhedra, magnetic anisotropy and the relaxation processes was investigated and discussed in detail.

Received 30th November 2019,
Accepted 18th December 2019

DOI: 10.1039/c9dt04592a

rsc.li/dalton

Introduction

Mononuclear Co(II) complexes showing slow magnetic relaxation are an attractive family of single-molecule magnets (SMMs),¹ due to the significant attention paid to the molecular magnets having only one metal centre, considerable anisotropy, and no intermetallic interactions, these molecules being named single-ion magnets (SIMs).² In general, the main characteristic feature of SMMs is the presence of magnetic hysteresis originating at the molecular level. Therefore the importance of these molecules relies on their potential applications

in molecular switches, sensors, spintronics and data storage nanotechnology.³ Magnetic bistability based on the hysteresis loop is related to the existence of the energy barrier of spin reversal (*U*). In the case of 3d-metal complexes, *U* is usually related to the zero-field splitting (ZFS)⁴ of the ground spin state as $U = |D|S^2$ for an even and $U = |D|(S^2 - 1/4)$ for an odd number of unpaired electrons in the valence shell of a metal ion, where *D* is the axial ZFS parameter defined within the spin Hamiltonian formalism. Thus, an interesting feature of SIMs lies in the probable prediction of magnetic anisotropy established from ligand field theory. In other words, the magnetic anisotropy of mononuclear complexes can be tuned by the rational design of the ligand field strength of the utilized ligands and their coordination geometry around the central atom.⁵

In parallel with the extensive study on lanthanide-based SIMs,⁶ Co(II) complexes are also excellent candidates for the synthesis of SIMs due to their high magnetic anisotropy and strong first order spin–orbit coupling among 3d metals.² The first two pentacoordinate mononuclear Co(II) complexes exhibiting slow-relaxation of magnetization reported by Jurca *et al.*⁷ inspired the further exploration of molecular magnetism in tetra-,⁸ penta-,⁹ hexa-¹⁰ or heptacoordinated¹¹ mononuclear Co(II) complexes. This chemistry is well-developed and in recent years it has continued to reveal new and interesting magnetic properties derived from the molecular geometry of these complexes. However, the goal-directed control in the syn-

^aDepartment of Inorganic Chemistry, Faculty of Chemical and Food Technology, Slovak University of Technology in Bratislava, Bratislava SK-81237, Slovakia.

E-mail: ivan.salitros@stuba.sk

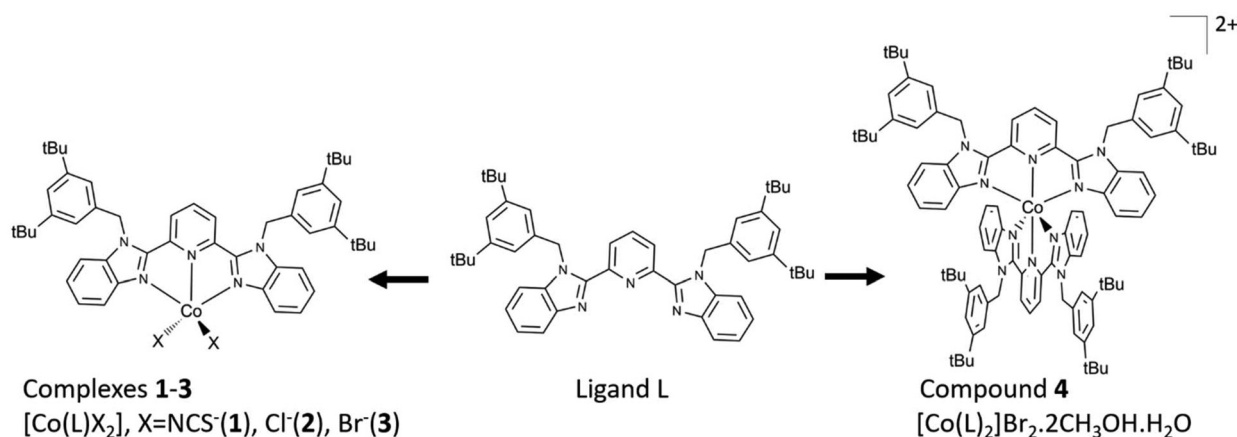
^bDepartment of Inorganic Chemistry, Faculty of Science, Palacký University, 17. listopadu 12, 771 46 Olomouc, Czech Republic

^cInstitut für Nanotechnologie, Karlsruher Institut für Technologie, Postfach 3640, Karlsruhe 76021, Germany

^dInstitute de Physique et Chimie de Matériaux de Strasbourg (IPCMS), CNRS-Université de Strasbourg, 23, rue du Loess, BP 43, 67034 Strasbourg cedex 2, France

^eCentral European Institute of Technology, Brno University of Technology, Purkyňova 123, 61200 Brno, Czech Republic

† Electronic supplementary information (ESI) available. CCDC 1888983–1888985 and 1954560. For ESI and crystallographic data in CIF or other electronic format see DOI: 10.1039/C9DT04592A



Scheme 1 Molecular structures of the tridentate ligand L, the neutral complexes **1–3** and the complex cation of compound **4**.

thesis of Co(II) complexes with a desired magnetic behaviour still remains a considerable challenge, and much more work is required to extend our knowledge of the structure–property relationship. In this context, the pentacoordinate Co(II) complexes with one rigid terpy-like tridentate ligand (terpy = 2,6-bis(2-pyridyl)pyridine) and two terminal ligand anions present an exciting family of field induced SIMs, where the correlation between the geometry of coordination polyhedra and the magnetic anisotropy might help to understand the impact of the molecular design on relaxation dynamics. Since the three bonds of the metal centre with a rigid N₃-donor ligand are fixed, the coordination polyhedron is usually affected by non-Berry Y or T angular distortion,¹² which also leads to the transformation of the trigonal bipyramid (TBPY, *D*_{3h}) to the square pyramid (SPY, *C*_{4v}), similar to the ideal Berry pseudo-rotation pathway. Based on the Addison parameter (τ_5),¹³ which quantitatively expresses the degree of interconversion between TBPY ($\tau_5 = 1$) and SPY ($\tau_5 = 0$), the majority of complexes reported to date in this family show an intermediate geometry between those two shapes, but often much closer to the latter.^{9b–d,14} In addition, it has been shown that the chemical nature of the two terminal ligand anions does not have a significant impact on the degree of TBPY–SPY interconversion^{9b–d} and TBPY geometry predominates only in the systems with flexible terpy-like N₃-donor ligands containing aliphatic spacers between the individual aromatic N-donor moieties.¹⁵ The axial ZFS parameter in such pentacoordinate Co(II) complexes with terpy-like N₃-donor ligands varies over a wide range from -41 to $+151$ cm⁻¹, and the magneto-structural correlation suggests the growing trend of *D* with a decreasing value of τ_5 .^{9b} On the other hand, hexacoordinated Co(II) complexes exhibit distorted octahedral geometry often influenced by interconversion to trigonal prism geometry (Bailar twist). This can lead to a huge magnetic anisotropy and hence large *U* as well.

The dynamic magnetic study of Co(II) complexes often proves the presence of field-induced slow relaxation, which at a high external static magnetic field ($B_{\text{DC}} > 0.2$ T) has occasionally multiple relaxation characters. The low-frequency relaxation channels with high relaxation times τ (10^0 – 10^{-2} s) are

usually based on the existence of intermolecular dipole–dipole interactions within the crystal lattice^{8–10,14,15} and can be suppressed by the decrease of the *B*_{DC} field. On the other hand, the fast relaxation channels are of pure molecular nature ($\tau \approx 10^{-4}$ – 10^{-9} s) and their analysis requires the combination of the Direct (AB^mT) + Orbach $\left(\frac{1}{\tau_0} \exp\left(-\frac{U_{\text{eff}}}{kT}\right)\right)$ or Direct (AB^mT) + Raman (CT^n) mechanism of spin reversal (*vide infra*, eqn (5)).^{10b} Apparently, the relaxation parameters *A*, τ_0 , *U*_{eff}, and *C* have an essential impact on the overall relaxation time τ at a given temperature, and therefore the understanding of their relationship with the structural features of Co(II) SIMs presents one of the pivotal challenges in this area of molecular magnetism.^{9b,d}

Herein we report four novel Co(II) SIMs containing a terpy-like N₃-donor aromatic ligand and pseudohalide or halide anions. Careful molecular design and goal-directed synthesis allowed us to prepare a derivative of the 2,6-bis(1*H*-benzimidazol-2-yl)pyridine ligand (L) functionalised with bulky 3,5-bis(*tert*-butyl)benzyl substituents (Scheme 1). The corresponding pentacoordinate Co(II) complexes **1** ($[\text{Co}(\text{L})(\text{NCS})_2]$), **2** ($[\text{Co}(\text{L})\text{Cl}_2]$) and **3** ($[\text{Co}(\text{L})\text{Br}_2]$) were prepared by variation of pseudohalido or halido terminal ligand anions, while compound **4** ($[\text{Co}(\text{L})_2]\text{Br}_2 \cdot 2\text{CH}_3\text{OH} \cdot \text{H}_2\text{O}$) contains a Co(II) metal centre in a pseudooctahedral environment. All four compounds were spectrally and structurally characterised and their static and dynamic magnetic properties allowed us to analyse ZFS parameters and slow relaxation mechanisms, respectively. Quantitative magnetic analysis was confronted with theoretical calculations at the CASSCF level, testing also the effects of different dynamic electron correlation methods (NEVPT2 *vs.* DCD-CAS(2)), the double-shell effect and the relativistic effects.

Results and discussion

Synthesis and structural investigation

The detailed synthetic procedures and characterisation of ligand L and reported complexes **1–4** are described in the

Experimental section (see the ESI†). The tridentate ligand L was prepared by reaction of 2,6-bis(1*H*-benzimidazol-2-yl)pyridine¹⁶ with 3,5-di-*tert*-butylbenzyl bromide in DMSO solution under basic conditions. Nucleophilic substitution afforded two products, which were successfully separated using column chromatography. The desired disubstituted ligand L was collected in 61% yield as the main product and the monosubstituted side-product L1 was obtained in 15% yield. The pentacoordinate complexes 1–3 were prepared in acetonitrile solution by complexation of ligand L with the corresponding Co(II) salt, which was used in small excess to prevent the formation of hexacoordinated complexes. Compound 4 was prepared in a methanol solution using a small excess of L to prevent the formation of a pentacoordinate complex (Scheme 1). The phase purity of the obtained polycrystalline materials was investigated by powder X-ray diffraction spectroscopy prior to all further spectroscopic and magnetic investigations (Fig. S1.5, see the ESI†). In order to investigate the dynamic magnetic properties of diluted compounds, we attempted to prepare Zn(II) doped complexes 1–4. However, in all four cases the synthesis ended up with the suspension of the dissolved corresponding Co(II) complex and the precipitated hexacoordinate Zn(II) complex, whose crystal symmetry in the case of doping of 4 does not match with the symmetry of the hexacoordinate Co(II) complex (Fig. S1.5d, see the ESI†).

Single crystal diffraction experiments confirmed the expected molecular structures of compounds 1–4 (Fig. 1) and selected crystallographic parameters are listed in Table 1. At 100 K, the pentacoordinate complexes 1–3 crystallise in the monoclinic *C2/c* (1) and *P2₁/c* (2 and 3) space groups and the asymmetric unit of each structure consists of one molecule of the neutral complex expressed by the general formula [Co(L)X₂] (X = NCS[−] for 1, Cl[−] for 2, and Br[−] for 3). Eight (1) and four (2 and 3) complex molecules are included in the respective unit cell and all three structures do not contain any lattice solvent molecules. Complexes 2 and 3 are isomorphic and isostructural to each other. Compound 4 crystallises in the triclinic *P1* space group and two asymmetric units expressed by the formula [Co(L)₂]Br₂·2CH₃OH·H₂O are present in the unit cell. The pentacoordinate Co(II) metal ion is surrounded by three nitrogen donor atoms of the tridentate ligand L, and the two remaining coordination sites are occupied either by the N donor atoms of the isothiocyanato ligand anion in 1 or by two halido anions Cl[−] and Br[−] in 2 and 3 (Fig. 1). Co–N distances formed between the central atom and the tridentate chelating ligand L vary in the narrow range of 2.092(2)–2.123(2) Å and their values indicate the high-spin state of the central atom (Fig. 1). The Co–N3 bond involving the pyridine nitrogen donor atom is shortened compared to the bonds formed by imidazole moieties (2.118(2) Å) in the coordination polyhedron 1, while the reverse situation is observed in the polyhedra of 2 and 3 (Fig. 1). It is interesting to note that the latter case found in 2 and 3 is predominant in the so far reported similar complexes and the elongation or shortening of the imidazole Co–N distances does not depend either on the type of terminal ligand or on the degree of interconversion between the square

planar and trigonal bipyramidal geometries of coordination polyhedra.^{9b} Furthermore, the lengths of coordination bonds, which involve the terminal ligands, strongly depend on the nature of the used anion X[−]. While isothiocyanato N-donor ligands form the shortest bonds within the coordination polyhedron of 1 (avg. 1.984(2) Å), the chlorido or bromido ligand anions form the weakest bonds in 2 and 3, respectively (avg. 2.2864(8) Å for 2; avg. 2.4358(9) Å for 3). The coordination geometries of 1–3 have been studied by the continuous symmetry measure methodology (program SHAPE 2.1),¹⁷ which provides a quantitative analysis of the deviation of a given shape of the coordination polyhedron. All three structures were compared to several ideal five-coordinated geometries (Table S2.1†)^{17c} among which the square pyramidal (SPY, *C_{4v}*) and/or vacant octahedral (vOC, *C_{4v}*) geometries are the closest for compound 1 (*S*(SPY) = 1.4 and *S*(vOC) = 2.1, respectively), while the trigonal bipyramidal geometry (TBPY, *D_{3h}*) is the closest for 2 (*S*(TBPY) = 2.0) and 3 (*S*(TBPY) = 2.5). The comparison of symmetry measures in the shape map (Fig. S2.1, see the ESI†) indicates that the Berry distortion between the ideal TBPY and SPY shapes is disrupted by another pathway, which most probably involves the vOC geometry. The coordination polyhedron of 1 with a rather SPY geometry contains a basal plane formed by N1, N3, N4 and N6 donor atoms, while the Co1–N7 bond represents the apical axis. Co(II) is pulled out from the basal plane and from the plane of the 2,6-bis(1*H*-benzimidazol-2-yl)pyridine moiety (*d* ≈ 0.4 Å and *d* ≈ 0.5 Å, respectively) towards the N7 vertex (Fig. S2.2a†) and most of the *cis* angles are significantly deviated from the ideal value of 90° (N3–Co1–N4 = 74.73(7)°; N4–Co1–N6 = 100.97(8)°; N6–Co1–N1 = 100.55(8)°; N1–Co1–N3 = 74.96(7)°; N7–Co1–N4 = 102.76(8)°; N7–Co1–N6 = 109.86(9)°). In contrast, the axial axis in the rather TPBY-shaped polyhedra of 2 and 3 involves both imidazole nitrogen donor atoms of L and along with the metal centre creates a significantly deviated angle from 180° (N1–Co1–N4 = 151.33(8)° for 2 and N1–Co1–N4 = 152.0(1)° for 3; Fig. S2.2b and c, see the ESI†). The equatorial plane is formed by the pyridine nitrogen donor atom N3 of L and two halido ligands, and the corresponding *cis* angles vary in the range of 111–127°, and thus they are close to the ideal angle of 120°. In both compounds, the Co(II) metal centres reside on the equatorial and on the ligand L planes (Fig. S2.2a and b, see the ESI†). Furthermore, the values of the τ₅ distortion parameter reflect the angular deviation of the coordination polyhedra in the reported compounds. Compared to the ideal values of τ₅ = 0 for SPY and τ₅ = 1 for TBPY, the τ₅ values (τ₅ = 0.30 for 1, τ₅ = 0.46 for 2 and τ₅ = 0.41 for 3) indicate an intermediate geometry between SPY and TBPY stereochemistry, however certainly disrupted by another geometry indicating the deviations from the ideal Berry pathway (Fig. S2.1, see the ESI†).

The ionic compound 4 contains a complex cation in which the Co–N distances of the coordination polyhedra vary from 2.08 Å with the pyridyl nitrogen atom to about 2.13 Å with the pyrazolyl moieties and are typical of the high-spin metal centre (Fig. 1d). The coordination environment of Co(II) formed by six nitrogen donor atoms of two tridentate ligands L

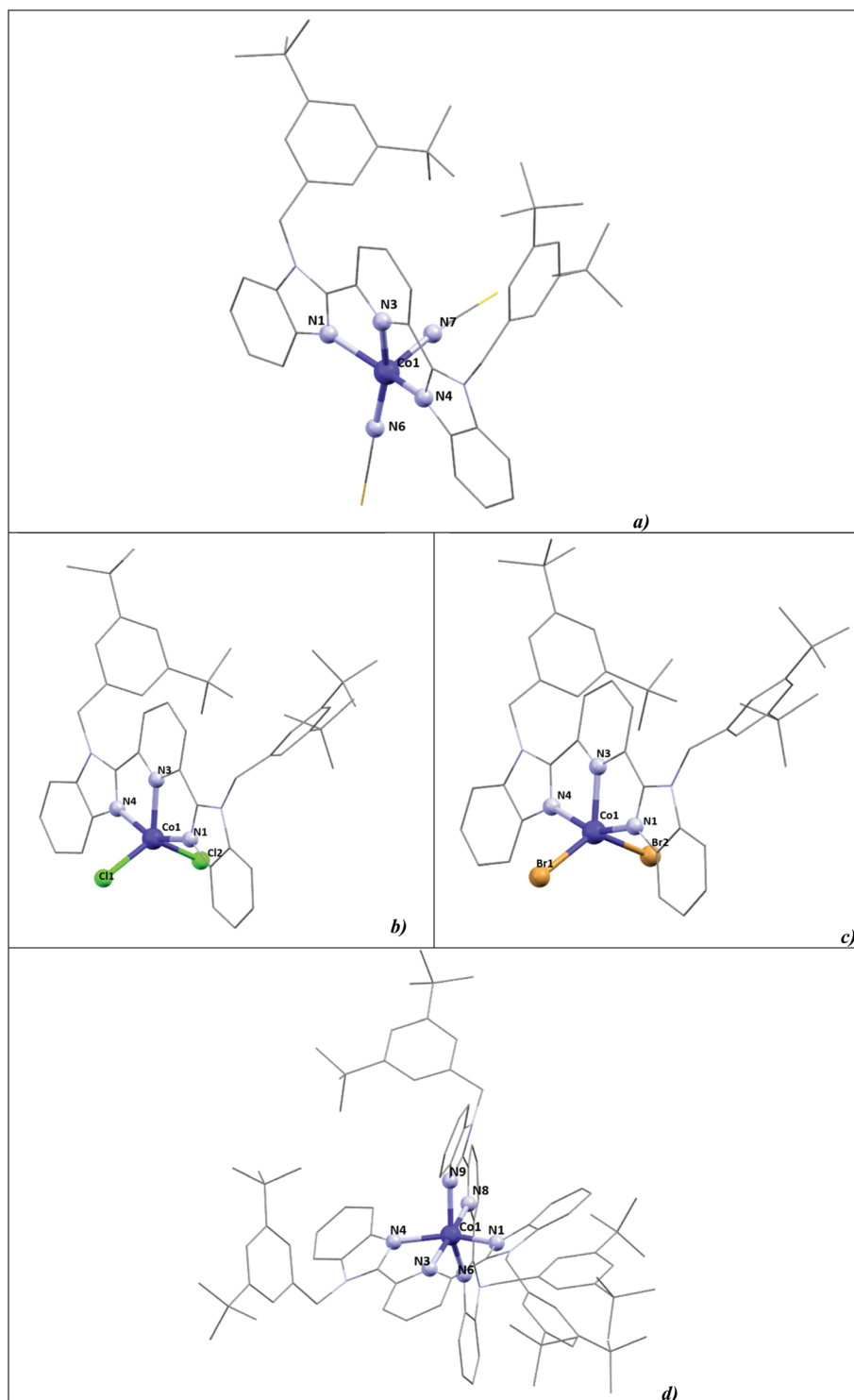


Fig. 1 Representation of the molecular structures of **1** (a), **2** (b), **3** (c) and **4** (d). Hydrogen atoms, uncoordinated anions and lattice solvent molecules are omitted for clarity. Colour code: C-grey; N-blue; Cl-green; Br-brown; S-yellow. Bond distances (in Å) and structural parameters of coordination polyhedra in **1**: Co1–N1 = 2.095(2), Co1–N3 = 2.118(2), Co1–N4 = 2.092(2), Co1–N6 = 1.964(2), Co1–N7 = 2.004(2), $S(\text{TBPY}) = 5.5$, $S(\text{SPY}) = 1.4$, $S(\text{vOC}) = 2.1$, $\tau_5 = 0.30(8)$; in **2**: Co1–N1 = 2.106(2), Co1–N3 = 2.105(2), Co1–N4 = 2.123(2), Co1–Cl1 = 2.3079(8), Co1–Cl2 = 2.2649(8), $S(\text{TBPY}) = 2.0$, $S(\text{SPY}) = 4.9$, $\tau_5 = 0.46(8)$; in **3**: Co1–N1 = 2.096(3), Co1–N3 = 2.088(3), Co1–N4 = 2.104(3), Co1–Br1 = 2.4639(8), Co1–Br2 = 2.4077(9), $S(\text{TBPY}) = 2.5$, $S(\text{SPY}) = 4.9$, $\tau_5 = 0.41(3)$; in **4**: Co1–N1 = 2.139(2), Co1–N3 = 2.081(2), Co1–N4 = 2.152(1), Co1–N6 = 2.119(2), Co1–N9 = 2.118(3), Co1–N8 = 2.084(2), $\Sigma = 136.4^\circ$.

Table 1 Selected crystallographic information for reported complexes 1–4

	1	2	3	4
Formula	C ₅₁ H ₅₇ CoN ₇ S ₂	C ₄₉ H ₅₇ Cl ₂ CoN ₅	C ₄₉ H ₅₇ Br ₂ CoN ₅	C ₁₀₀ H ₁₂₄ Br ₂ CoN ₁₀ O ₃
Formula weight/g mol ⁻¹	891.08	845.82	934.74	1732.83
Crystal colour	Green	Brownish green	Orange	Orange
Temperature/K	100	100	100	100
Wavelength/Å	1.54186	1.54186	1.54186	1.54186
Crystal system	Monoclinic	Monoclinic	Monoclinic	Triclinic
Space group	C2/c	P2 ₁ /c	P2 ₁ /c	P $\bar{1}$
<i>a</i> /Å	37.1120(8)	17.9448(4)	17.9513(4)	13.5981(4)
<i>b</i> /Å	15.8626(2)	8.89550(10)	8.8923(2)	18.2954(5)
<i>c</i> /Å	17.1798(4)	30.1258(6)	30.3407(7)	21.4975(6)
α /°	90	90	90	67.463(2)
β /°	90.502(2)	97.649(2)	97.413(2)	87.059(2)
γ /°	90	90	90	72.737(2)
<i>V</i> /Å ³	10 113.2(3)	4766.13(15)	4802.75(19)	4705.4(2)
<i>Z</i> ; ρ_{calc} /g cm ⁻³	8; 1.170	4; 1.179	4; 1.293	2; 1.223
μ (Cu-K α)/mm ⁻¹	3.732	4.128	5.023	2.836
<i>F</i> (000)	3768.0	1788	1932	1830.0
Crystal size/mm	0.15 × 0.09 × 0.02	0.32 × 0.25 × 0.03	0.21 × 0.15 × 0.02	0.45 × 0.25 × 0.15
θ range for the data collection/°	6.06 to 142.712	7.206 to 143.908	5.874 to 142.818	2.23 to 71.67
Final <i>R</i> indices [<i>I</i> > 2 σ (<i>I</i>)] ^a	<i>R</i> ₁ = 0.0438, <i>wR</i> ₂ = 0.1037	<i>R</i> ₁ = 0.0482, <i>wR</i> ₂ = 0.1146	<i>R</i> ₁ = 0.0439, <i>wR</i> ₂ = 0.0902	<i>R</i> ₁ = 0.0378, <i>wR</i> ₂ = 0.0944
<i>R</i> indices (all data) ^a	<i>R</i> ₁ = 0.0685, <i>wR</i> ₂ = 0.1125	<i>R</i> ₁ = 0.0742, <i>wR</i> ₂ = 0.1224	<i>R</i> ₁ = 0.0810, <i>wR</i> ₂ = 0.0948	<i>R</i> ₁ = 0.0502, <i>wR</i> ₂ = 0.0977
GoF on <i>F</i> ²	0.918	0.857	0.861	0.933
CCDC deposit number	1888985	1888983	1888984	1954560

$$^a R_1 = \sum (F_o - F_c) / \sum (F_o); \quad wR_2 = \sqrt{\sum [w(F_o^2 - F_c^2)^2] / \sum [w(F_o^2)^2]}.$$

shows a pronounced distortion from a perfect octahedral geometry, which can be quantitatively expressed by several angles and parameters postulated mainly for the identification of the spin state of the central atom but also for the quantification of Jahn–Teller distortion.¹⁸ For instance, the *trans* angle N3–Co1–N8 involving two pyridine N_{py} donor atoms ϕ , the dihedral angle between the least-squares planes of the two L ligand moieties coordinating with the same metal centre θ , the two clamp angles φ (N1–Co–N4 and N6–Co–N9) and the four bite angles α (N_{im}–Co–N_{py}) (Fig. S2.3a and b, see the ESI†) would acquire 90° (θ , α) and 180° (ϕ , φ), respectively, if the coordination polyhedron {CoN₆} shows an ideal octahedral symmetry. Moreover, the angular distortion parameters Σ ¹⁸ calculated from the 12 *cis* angles of the hexacoordinated polyhedron (Fig. S2.3c, see the ESI†) acquiring zero values when ideal octahedral symmetry is present are suitable indicators of octahedral deviation. All the above-mentioned angles indicate severe divergence from the values of the ideal octahedral shape ($\phi = 174.69(7)^\circ$, $\varphi_{\text{avg}} = 152.17(8)^\circ$, $\theta = 82.94(8)^\circ$ and $\alpha_{\text{avg}} = 76.19(2)^\circ$) and along with $\Sigma = 136.4^\circ$ they reflect a pronounced degree of angular distortion in [Co(L)₂]²⁺. In addition, those values are typical of high-spin hexacoordinated Co(II) complexes with terpy-like N₃-donor ligands, while for comparison, the typical values of the less distorted low-spin polyhedra of that family are $\phi \approx 176^\circ$, $\varphi \approx 160^\circ$, $\theta \approx 86^\circ$, $\alpha \approx 80^\circ$ and $\Sigma \approx 90^\circ$.¹⁹

In the crystal structures of 1–3, the two 3,5-bis(*tert*-butyl)phenyl moieties of L are bent in the same direction with respect to each other, creating an angle of about $\approx 115^\circ$ with respect to the 2,6-bis(1*H*-benzimidazol-2-yl)pyridine plane (Fig. S2.3 and S2.4, see the ESI†) and present steric constraints

on that side of the ligand moiety. Therefore, the non-covalent interactions between the pyridine and benzimidazole parts of the neighbouring molecules are observed only on the “free” side in which the bulky aromatic substituents are not directed. In the crystal lattice of 2 and 3, it is therefore possible to recognise the formation of pseudodimeric couples, where two complex molecules are interconnected through weak π – π contacts formed between the benzimidazole moieties ($d \approx 3.6$ Å for 2 and 3; Fig. S2.4b and c, see the ESI†). Those neighbouring pseudodimeric couples are bent with respect to each other by an angle of $\approx 148^\circ$ in 2 and $\approx 145^\circ$ in 3 and are aligned along the *b*–*c* plane. The crystal structure of 1 shows similar pseudodimeric couples along the *a*–*c* plane, which are however interconnected *via* weak π – π interactions between the pyridine and benzimidazole moieties of two neighbouring molecules ($d \approx 3.3$ Å; Fig. S2.4a, see the ESI†). In the complex cation of 4, the 3,5-bis(*tert*-butyl)phenyl substituents are oriented in the opposite direction to each other preventing the formation of relevant non-covalent interactions within the crystal lattice (Fig. 1d).

Static magnetic properties and theoretical calculations

To gain more insight into the magnetic anisotropy of the reported complexes 1–4, static magnetic data were acquired and further analysed – see Fig. 2. The temperature dependent magnetic data, shown as the effective magnetic moments, clearly reveal substantial zero-field splitting (ZFS) causing the decrease of μ_{eff} upon lowering the temperature. This phenomenon is also responsible for much lowered saturation values of the isothermal magnetizations measured at $T = 2$ K in com-

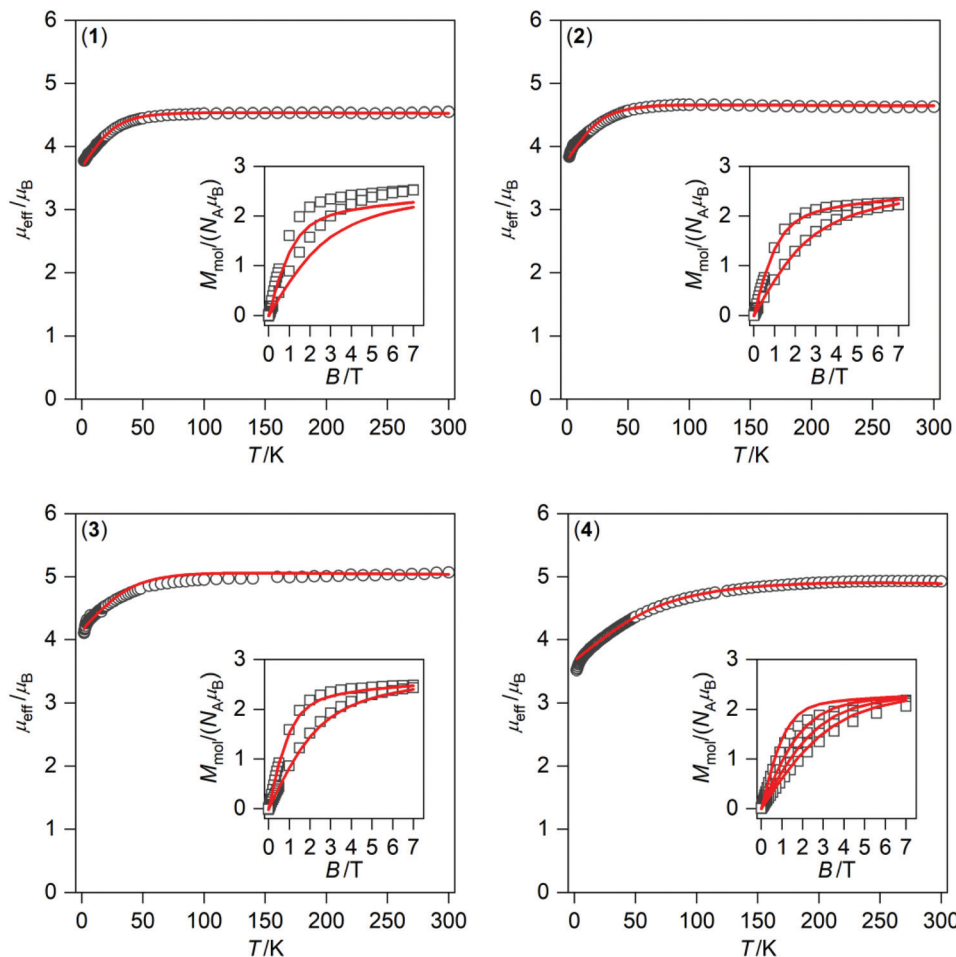


Fig. 2 Magnetic data for 1–4 shown as the temperature dependence of the effective magnetic moment and as the isothermal magnetizations in the insets. The empty symbols represent the experimental data and red solid lines represent the fitted data using eqn (1) or (4) with the parameters listed in Table 2.

parison with the theoretical values $M_{\text{mol}}/N_A\mu_B = g \cdot S \approx 3$ for $S = 3/2$ and $g = 2.0$.

Therefore, the obtained temperature dependent magnetization data and the field dependent magnetization data at different temperatures were analysed simultaneously using spin Hamiltonian covering the zero-field splitting terms and Zeeman term defined as

$$\hat{H} = D(\hat{S}_z^2 - \hat{S}^2/3) + E(\hat{S}_x^2 - \hat{S}_y^2) + \mu_B B g \hat{S}_a \quad (1)$$

where D and E are the single-ion axial and rhombic ZFS parameters, respectively, and the last component is the Zeeman term defined in the direction of the magnetic field as $B_a = B(\sin(\theta)\cos(\varphi), \sin(\theta)\sin(\varphi), \cos(\theta))$ with the help of the polar coordinates.²⁰ Next, the molar magnetization (M_{mol}) was calculated from the partition function (Z) for the given direction of magnetic field B_a as

$$M_{\text{mol}} = N_A \frac{d \ln Z}{dB_a} \quad (2)$$

Then, the integral (orientational) average of molar magnetization was calculated as

$$M_{\text{mol}} = 1/4\pi \int_0^{2\pi} \int_0^\pi M_a \sin \theta d\theta d\varphi \quad (3)$$

to properly simulate experimental powder magnetization data for all temperature and magnetic field dependent experimental data. The *ab initio* calculations performed on the complexes (*vide infra*) suggest positive D parameters and large g -anisotropy with the g_z component close to 2.0. Thus, the g_z component of the g -tensor was fixed to a value of 2.0 in order to minimize the number of optimized parameters. The best-fits were obtained for 1–3 with D in the range from 25 to 39 cm^{-1} and significant rhombicity (Table 2). However, this approach was unsuccessful for compound 4 with pseudo-octahedral geometry of the coordination polyhedron. Hence, we used the second approach suitable for such a scenario based on the reports of Griffith,²¹ Lines²² and Figgis,²³ in which the orbital

Table 2 Spin Hamiltonian parameters calculated by *ab initio* methods and fitted from the magnetic data for 1–4

	[Co(L)(NCS) ₂] of 1	[Co(L)Cl ₂] of 2	[Co(L)Br ₂] of 3	[Co(L') ₂] ²⁺ of 4 ^a
CASSCF/NEVPT2 with CAS(7,5) using def2-TZVP(Co, Br, Cl, N, S) and def2-SVP(C,H)				
<i>D</i> (cm ⁻¹)	28.8	48.0	49.1	63.8
<i>E/D</i>	0.311	0.117	0.226	0.133
<i>g_x</i>	2.319	2.402	2.346	2.444
<i>g_y</i>	2.573	2.544	2.627	2.630
<i>g_z</i>	2.098	1.991	2.082	1.985
Analysis of ground state Kramers doublets with an effective spin 1/2:				
<i>g₁</i> ^b	1.608	1.926	1.914	2.028
<i>g₂</i>	2.460	3.920	3.061	3.840
<i>g₃</i>	6.924	5.889	6.688	6.156
<i>g_{aver}</i>	3.664	3.912	3.888	4.008
CASSCF/NEVPT2 with CAS(7,10) using def2-TZVP(Co, Br, Cl, N, S) and def2-SVP(C,H) (double shell effect)				
<i>D</i> (cm ⁻¹)	29.7	50.6	55.4	63.6
<i>E/D</i>	0.314	0.124	0.219	0.124
<i>g_x</i>	2.333	2.423	2.314	2.452
<i>g_y</i>	2.601	2.591	2.675	2.631
<i>g_z</i>	2.098	1.989	2.142	1.974
CASSCF/NEVPT2/ZORA with CAS(7,5) using ZORA-def2-TZVP(Co, Br, Cl, N, and S) and ZORA-def2-SVP(C and H) (relativistic effects)				
<i>D</i> (cm ⁻¹)	27.9	47.6	49.3	62.0
<i>E/D</i>	0.300	0.119	0.231	0.133
<i>g_x</i>	2.318	2.400	2.337	2.437
<i>g_y</i>	2.560	2.544	2.634	2.620
<i>g_z</i>	2.098	1.991	2.091	1.984
CASSCF/DCD-CAS(2) with CAS(7,5) using def2-TZVP(Co, Br, Cl, N and S) and def2-SVP(C and H) (different treatments of dynamic electron correlation)				
<i>D</i> (cm ⁻¹)	30.0	50.1	55.0	64.3
<i>E/D</i>	0.309	0.125	0.235	0.120
Fitted parameters from the experimental magnetic data				
<i>D</i> (cm ⁻¹)	24.7	26.0	39.2	$\Delta_{\text{ax}} = 307 \text{ cm}^{-1}$
<i>E/D</i>	0.333	0.333	0.333	$\Delta_{\text{rh}}/\Delta_{\text{ax}} = 0.00$
<i>g_{xy}</i>	2.48	2.56	2.82	$\lambda = -121 \text{ cm}^{-1}$
<i>g_z</i>	2.00	2.00	2.00	$\alpha = 1.29$

^a L' is the simplified ligand L in which the *tert*-butyl groups were replaced by hydrogen atoms. ^b The *g*-parameters calculated for the ground state Kramers doublet with an effective spin $S_{\text{eff}} = 1/2$.

angular momentum and spin-orbit coupling are included in the Hamiltonian as

$$\hat{H} = -\alpha \cdot \lambda (\vec{S} \cdot \vec{L}) + \Delta_{\text{ax}} (\hat{L}_z^2 - \hat{L}^2/3) + \Delta_{\text{rh}} (\hat{L}_x^2 - \hat{L}_y^2) + \mu_{\text{B}} \vec{B} (g_e \vec{S} - \alpha \vec{L}) \quad (4)$$

where Δ_{ax} and Δ_{rh} describe the splitting of the $^4\text{T}_{1\text{g}}$ ground term induced by lowering the symmetry, α is the orbital reduction factor, λ is the spin-orbit coupling parameter and $g_e = 2.0023$. This L-S Hamiltonian exploits the T_1 - P isomorphism, and thus, the angular orbital momentum L is equal to 1 with the effective Landé *g*-factor, $g_L = -\alpha$, and is applied to $|S, L, M_S, M_L\rangle$ functions with $M_L = 0, \pm 1$ and $M_S = \pm 1/2, \pm 3/2$.²⁴ The orbital reduction factor combines two parameters, $\alpha = A\kappa$, where A is the Figgis coefficient of the configuration interaction resulting from the admixture of the excited terms reflecting the ligand field strength ($1 < A < 3/2$), and κ describes the lowering orbital contribution due to the covalency of the metal-ligand bond and it usually holds $\kappa \leq 1$. In addition, the spin-orbit coupling parameter λ can also be reduced in comparison with its free-ion value $\lambda_0 = -180 \text{ cm}^{-1}$ due to the covalent character of the donor-acceptor bond. The Hamiltonian in eqn (4) was able to properly describe the mag-

netic data for 4 using these best-fit parameters: $\Delta_{\text{ax}} = 307 \text{ cm}^{-1}$ and $\Delta_{\text{rh}}/\Delta_{\text{ax}} = 0.00$ with $\lambda = -121 \text{ cm}^{-1}$ and $\alpha = 1.29$ (Fig. 2).

In the next step, the multireference *ab initio* calculations based on the state-averaged complete active space self-consistent field method (SA-CASSCF) were conducted to gain insight into the electronic structure of the Co(II) ions in the studied compounds 1–4. Thus, the well-established ORCA software package²⁵ was used for these CASSCF calculations with the active space defined as seven electrons in five d-orbitals, CAS(7,5). In addition, dynamic electronic correlation was investigated by using the N-electron valence state perturbation theory (NEVPT2).²⁶ These calculations were performed on the mono-nuclear molecular fragments extracted from the experimental X-ray structures of 1–4. In the case of the complex cation of 4, the *tert*-butyl groups were replaced by hydrogen atoms to make such calculations feasible. Subsequently, the atomic positions of all hydrogen atoms were optimized using the PBE functional²⁷ together with the atom-pairwise dispersion correction method (D3BJ).²⁸ The results of CASSCF/NEVPT2 calculations are summarized in Table 2 and Fig. 3 and 4.

Generally, in an ideal square-pyramidal arrangement, the d-orbitals are split into d_{xy} , (d_{xz} , d_{yz}), d_{z^2} , and $d_{x^2-y^2}$ patterns, whereas the ideal trigonal-bipyramidal arrangement results in (d_{xz} , d_{yz}), (d_{xy} , $d_{x^2-y^2}$), and d_{z^2} patterns (Fig. S3.1, see the ESI†),

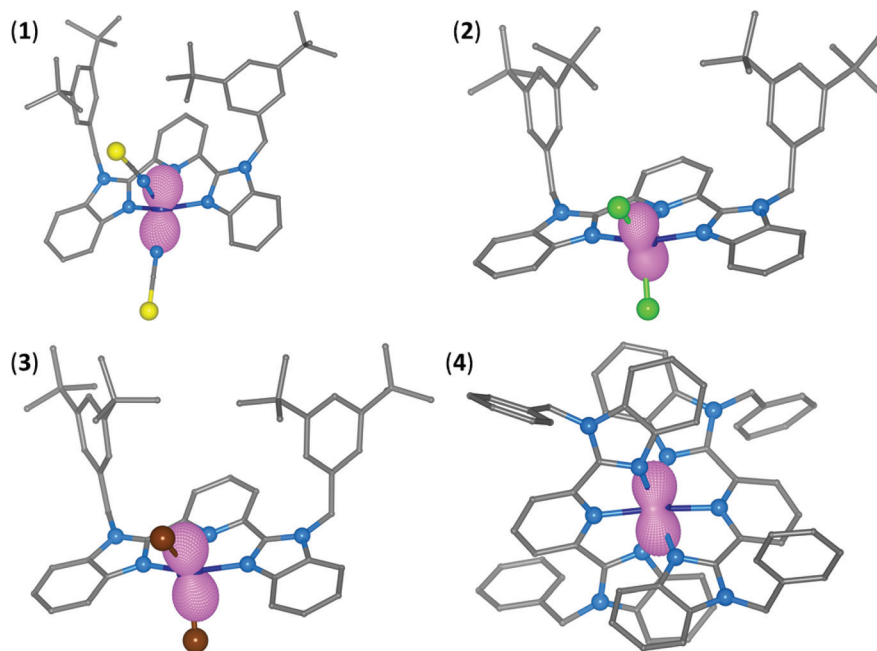


Fig. 3 Three-dimensional (3D) representation of molar magnetization (M_{mol}) calculated for $T = 2$ K and $B = 0.5$ T using CASSCF/NEVPT2 calculation with CAS(7,5) overlaid over the molecular fragments of 1–4.

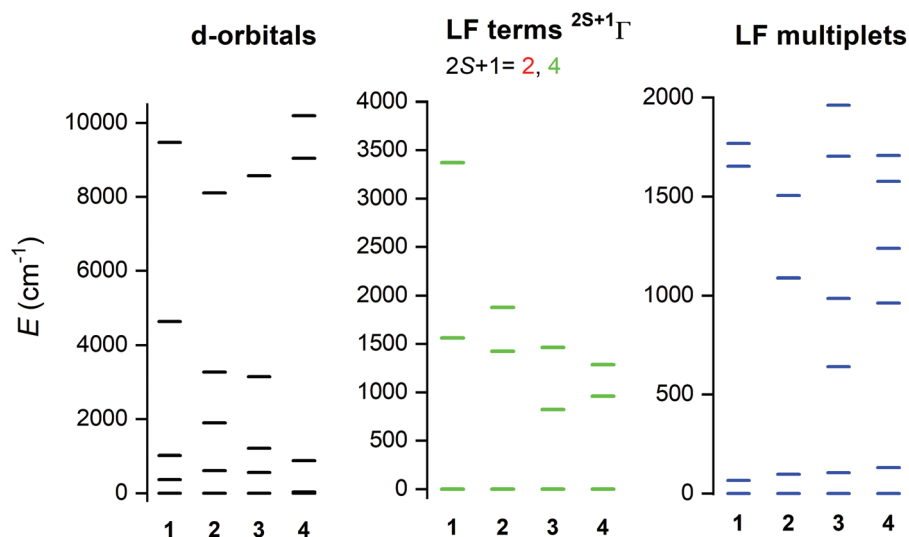


Fig. 4 The graphical output of the CASSCF/NEVPT2 calculations with CAS(7,5) for the mononuclear molecular fragments of 1–4. Plot of the d-orbitals splitting calculated by *ab initio* ligand field theory (AILFT)²⁹ utilized to calculate the energy of the d-orbitals in 1–4 as depicted in Fig. 4 (left). In the case of complexes 1 and 2, the d-orbital splitting resembles the one obtained for the square-pyramidal arrangement and trigonal-bipyramidal arrangement, respectively. Complex 3 showed the d-orbital splitting somewhere between these two cases, which is in agreement with the results of the geometry characterization done by using the SHAPE program. As expected, two sets of split t_{2g} and e_g orbitals were found in the pseudo octahedral complex 4. Subsequently, the CASSCF/NEVPT2 lowest ligand field terms are shown in Fig. 4 (middle) confirming the ground state with multiplicity four and low-lying excited terms, which have the largest contributions to the D -tensor (Table S3.1, see the ESI†). Next, due to spin-orbit coupling, the ligand-field terms (LFT) are split into the ligand-field multiplets (LFM) showing the zero-field splitting into several Kramers doublets – Fig. 4 (right). The application of

which can be confronted with the results obtained by the *ab initio* ligand field theory (AILFT)²⁹ utilized to calculate the energy of the d-orbitals in 1–4 as depicted in Fig. 4 (left). In the case of complexes 1 and 2, the d-orbital splitting resembles the one obtained for the square-pyramidal arrangement and trigonal-bipyramidal arrangement, respectively. Complex 3 showed the d-orbital splitting somewhere between these two cases, which is in agreement with the results of the geometry characterization done by using the SHAPE program. As

expected, two sets of split t_{2g} and e_g orbitals were found in the pseudo octahedral complex 4. Subsequently, the CASSCF/NEVPT2 lowest ligand field terms are shown in Fig. 4 (middle) confirming the ground state with multiplicity four and low-lying excited terms, which have the largest contributions to the D -tensor (Table S3.1, see the ESI†). Next, due to spin-orbit coupling, the ligand-field terms (LFT) are split into the ligand-field multiplets (LFM) showing the zero-field splitting into several Kramers doublets – Fig. 4 (right). The application of

the effective Hamiltonian theory³⁰ to a quartet ground state resulted in the ZFS D and E parameters and g -tensor parameters which are summarized in Table 2. Positive D is found for all complexes 1–4, with the smallest value found for 1 and the largest for 4. The calculated principal axes of the D -tensor are depicted in Fig. S3.2.† The positive D would result in the easy-plane type magnetic anisotropy, however, a larger E/D ratio suggests that the easy-axis type of magnetic anisotropy can be operative,³¹ and indeed, the calculated three-dimensional molar magnetization for 1–4 using CASSCF/NEVPT2 calculations nicely showed the axial character of the magnetic anisotropy in 1–4 (Fig. 3). This can be quantitatively analysed by using effective spin $S_{\text{eff}} = 1/2$ spin Hamiltonian for the ground state Kramers doublet, which results in three values of the effective g -factors (g_1 , g_2 and g_3) with their average value g_{aver} . If it holds that $g_1, g_2 < g_{\text{aver}}$ and $g_{\text{aver}} < g_3$, the easy-axis type of magnetic anisotropy of the ground state is present. In contrast, the easy-plane type of magnetic anisotropy is achieved under conditions $g_1 < g_{\text{aver}}$ and $g_{\text{aver}} < g_2, g_3$. These values are listed in Table 2, and it can be deduced that the easy-axis type of magnetic anisotropy is found in complexes 1, 3 and 4.

Moreover, the double-shell effect, which is supposed to be important for late 3d-metals, was accounted for by enlarging the active space to 10 d-orbitals (3d + 4d). Interestingly, this approach (CAS(7,5) vs. CAS(7,10)) has only a minor impact on the derived D and E ZFS parameters and g -factors (Table 2). Furthermore, we were interested if the relativistic effect may lead to different results, at least for complex 2 with coordinated bromide ligands. Therefore, ZORA (the 0th order regular approximation)³² relativistic correction was applied together with the relativistic version of the respective basis sets for CAS(7,5), but the results are almost identical to the non-relativistic calculations. Finally, we explored the recently introduced different approach to treat the dynamic electron correlation, 2nd order dynamic correlation dressed CAS, DCD-CAS (2) again for CAS(7,5).³³ This method led to slightly larger values of D -parameters for all complexes. Thus, we may conclude that all four tested approaches provided similar information about the electronic structure and large magnetic anisotropy is present in complexes 1–4.

Dynamic magnetic experiments

The magnetic data induced by the oscillating, alternating-current (AC) magnetic field were obtained at an amplitude of $B_{\text{AC}} = 0.38$ mT (1 and 3) and $B_{\text{AC}} = 0.35$ mT (2 and 4). The DC field scan for a limited number of frequencies over four orders of magnitudes shows that the out-of-phase component (χ'') of AC susceptibility is silent at $B_{\text{DC}} = 0$ T (Fig. S4.1†). This indicates very fast relaxation of the magnetization, probably due to the quantum tunnelling of magnetization (QTM) induced by hyperfine interactions with the nuclear spin and/or dipolar interactions between the spin centres in the lattice. In order to determine the optimum DC field to suppress the QTM effect, AC susceptibility measurements under various DC fields were applied at 2 K (Fig. S4.1†). Upon increasing the DC field up to $B_{\text{DC}} = 0.5$ T, the out-of-phase component varies, but differently

for individual frequencies. This confirms that compounds 1–4 show field-induced slow magnetic relaxation and therefore the subsequent temperature and frequency dependent measurements were carried out by choosing B_{DC} fields at which the out-of-phase components χ'' reach the maximal response ($B_{\text{DC}} = 0.15$ T for compounds 1 and 2, $B_{\text{DC}} = 0.1$ T for 4 and $B_{\text{DC}} = 0.125$ T for 3). Furthermore, in order to get detailed information about the both relaxation channels of compound 3 (*vide infra*), another three measurements were performed at $B_{\text{DC}} = 0.05$ T, $B_{\text{DC}} = 0.2$ T, and $B_{\text{DC}} = 0.3$ T. The collected sets of χ' and χ'' susceptibilities at each temperature were fitted using the formulas for the one-set (1, 2, 4, and 3 at 0.05 T and 3 at 0.125 T; eqn (S1) and (S2) see the ESI†) or two-set (3 at 0.2 T and 3 at 0.3 T; eqn (S3) and (S4) see the ESI†) Debye model.

Frequency dependent in-phase χ' and out-of-phase susceptibility χ'' measured as a function of frequency of the AC field for a set of temperatures (1.8–4.9 K for 1; 2.0–3.6 K for 2; Fig. 5a and b, Fig. S4.2 and S4.3, see the ESI†) suggest a single relaxation process in compounds 1 and 2. However, the small onsets apparent at very low frequencies in the χ'' vs. ν dependencies (Fig. 5a and b) indicate that both compounds contain the second relaxation channel which will become more pronounced at higher fields and lower temperatures. The out-of-phase components of AC susceptibility (χ'') show the maxima shift from 76.3 Hz (1 at 1.8 K, $\tau = 2.09$ ms) and from 331.6 Hz (for 2 at 2.0 K, $\tau = 0.48$ ms), respectively, to higher frequencies upon the increase of the temperature (Tables S4.2 and S4.3†). This indicates the typical features of SMMs – the maxima of χ'' are frequency and temperature dependent and the relaxation time τ shortens with the increase of temperature. The in-phase (χ') and out-of-phase (χ'') components of AC susceptibility were simultaneously fitted using the one-set Debye model, by which the adiabatic χ_S and isothermal χ_T susceptibilities along with the distribution parameter α_i and relaxation time τ_i were determined by nonlinear optimisation (eqn (S1) and (S2), see the ESI†). Using these parameters, interpolation/extrapolation lines enable us to reconstruct the frequency dependent AC susceptibility components (solid lines in Fig. 5 and in Fig. S4.2a and S4.3a, see the ESI†) and the arcs in the Argand (Cole–Cole) plot (Fig. S4.2b and S4.3b, see ESI†). The fitting procedure was terminated at $T = 4.9$ K (1) or 3.6 K (2), since the maxima for the relaxation channel already lie outside the hardware limits above those temperatures. Both measurements allow a reliable analysis of $\tau(T)$ dependency according to the extended relaxation equation

$$\frac{1}{\tau} = \frac{1}{\tau_0} \exp\left(-\frac{U}{kT}\right) + CT^m + AB^mT \quad (5)$$

where the corresponding terms describe the thermally activated Orbach $\left(\frac{1}{\tau_0} \exp\left(-\frac{U}{kT}\right)\right)$, Raman (CT^m) and direct (AB^mT) relaxation of magnetization. Usually, the first two terms describe the spin relaxation at higher temperature and the obtained parameters from the single Orbach or single Raman mechanism fitting help to estimate the extrapolated relaxation time τ_0 (for $T \rightarrow$ infinity), energetic barrier of spin

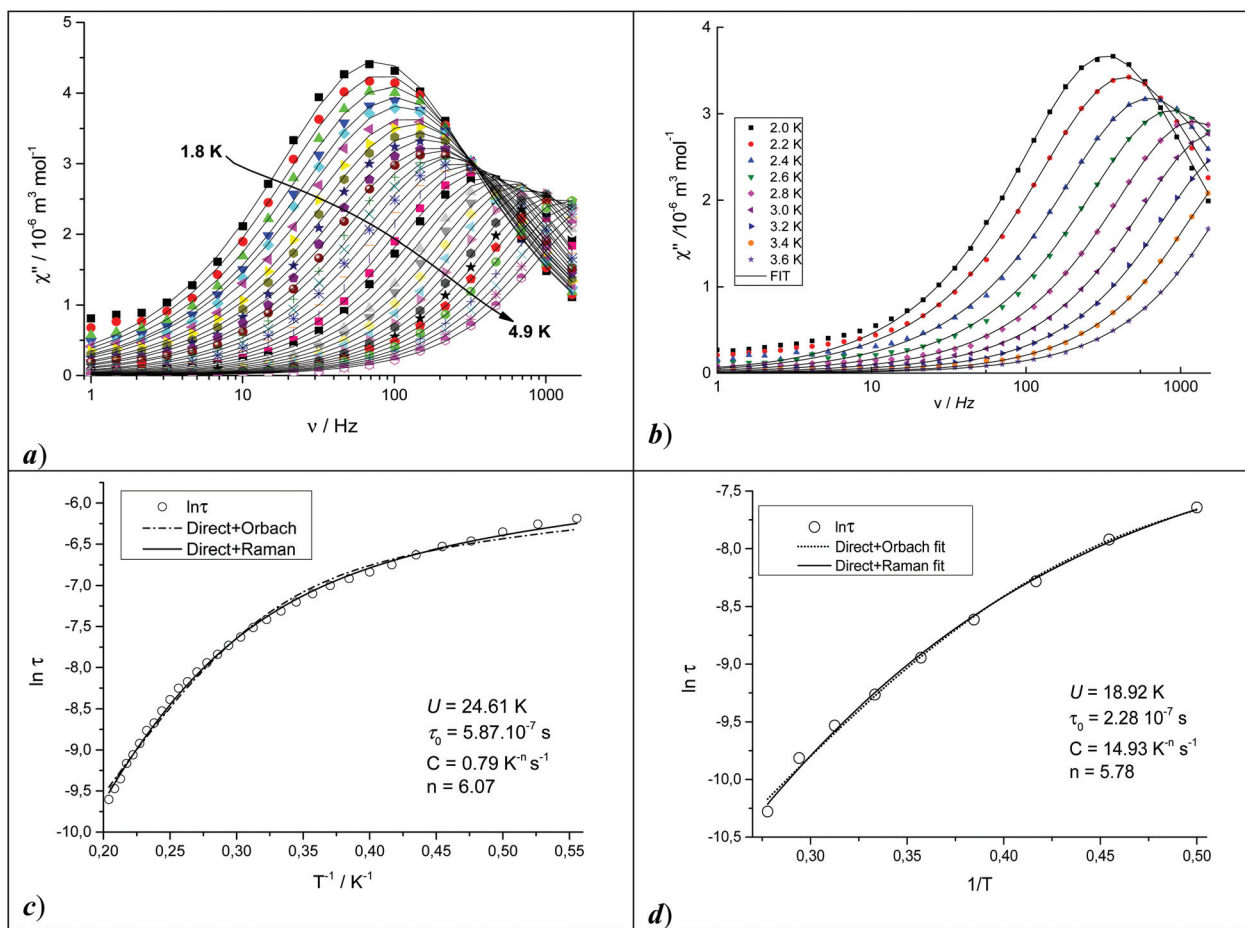


Fig. 5 Frequency dependent out-of-phase χ'' components of AC susceptibility for **1** (a) and **2** (b) at the applied external magnetic field $B_{DC} = 0.15$ T. Solid lines represent the fits using the one-component Debye model (eqn (S1) and (S2); see the ESI†). The fits of the resulting relaxation times τ with the combination of the Orbach and direct processes (solid lines) using eqn (5) and the combination of the Raman and direct processes (dashed lines) using eqn (5) for **1** (c) and **2** (d).

reversal U , or coefficients of the Raman term (C , n) for the combined fitting models (Orbach + direct or Raman + direct, Fig. 5c and d). The best fit parameters are listed in Table S4.6 (see the ESI†). In the case of the combined Orbach + direct model, the energy barrier and extrapolated relaxation times $U = 24.6$ K, $\tau_0 = 5.9 \times 10^{-7}$ s for **1** and $U = 18.9$ K, $\tau_0 = 2.3 \times 10^{-7}$ s for **2**, respectively, are typical of the pentacoordinate Co(II) SIMs. The values of the Raman parameter C (0.79 K $^{-n}$ s $^{-1}$ for **1** and 14.93 K $^{-n}$ s $^{-1}$ for **2**) extracted from the Raman + direct model suggest that two-phonon Raman relaxation is more pronounced in compound **2**. The Raman exponent acquires a value close to $n \approx 6$ for both compounds **1** and **2**, which is smaller than the expected value of 9 for Kramers ions,³⁴ but when optical and acoustic phonons are considered, $n = 1$ –6 is reasonable.³⁵ Both fitting approaches afforded comparable values of the AB^m parameter of the single-phonon direct relaxation mechanism (Table S4.6†).

Dynamic magnetic properties of **3** indicate the presence of two relaxation channels (Fig. 6a, b and Fig. S4.4–S4.7†), and therefore AC susceptibility was measured at four different static magnetic fields to investigate both low-frequency (LF) and

high-frequency (HF) channels at higher fields analysed by using the two-component Debye model (eqn (S3) and (S4), see the ESI†) and a single HF process at lower B_{DC} processed by the one-component Debye model (eqn (S1) and (S2), see the ESI†). The slower LF channel gains the maximum of χ'' at 5.70 Hz ($\tau_1 = 27.5$ ms, 0.2 T) and at 5.45 Hz ($\tau_1 = 29.2$ ms, 0.3 T) and the relaxation time is rather temperature invariant upon the increase of temperature (Fig. 6d and Table S4.4†). Since the appearance of the LF relaxation channel vanishes in the sample dispersed with the diamagnetic eicosane (Fig. S4.9, see the ESI†), its origin can be attributed to the existence of intermolecular dipole–dipole interactions always present in molecular systems. Those interactions are responsible for the formation of “finite oligomers” (finite chains, plates, blocks, or other fragments), with the coherence length depending upon temperature. The magnetic field raises the efficiency of the LF relaxation mode which points to its intermolecular nature, supported by the magnetic field. Moreover, the relaxation time for the LF mode is prolonged as the magnetic field increases.

The analysis of $\tau_2(T)$ of the HF channel of **3** was done in the same way as for compounds **1** and **2**. The use of the single

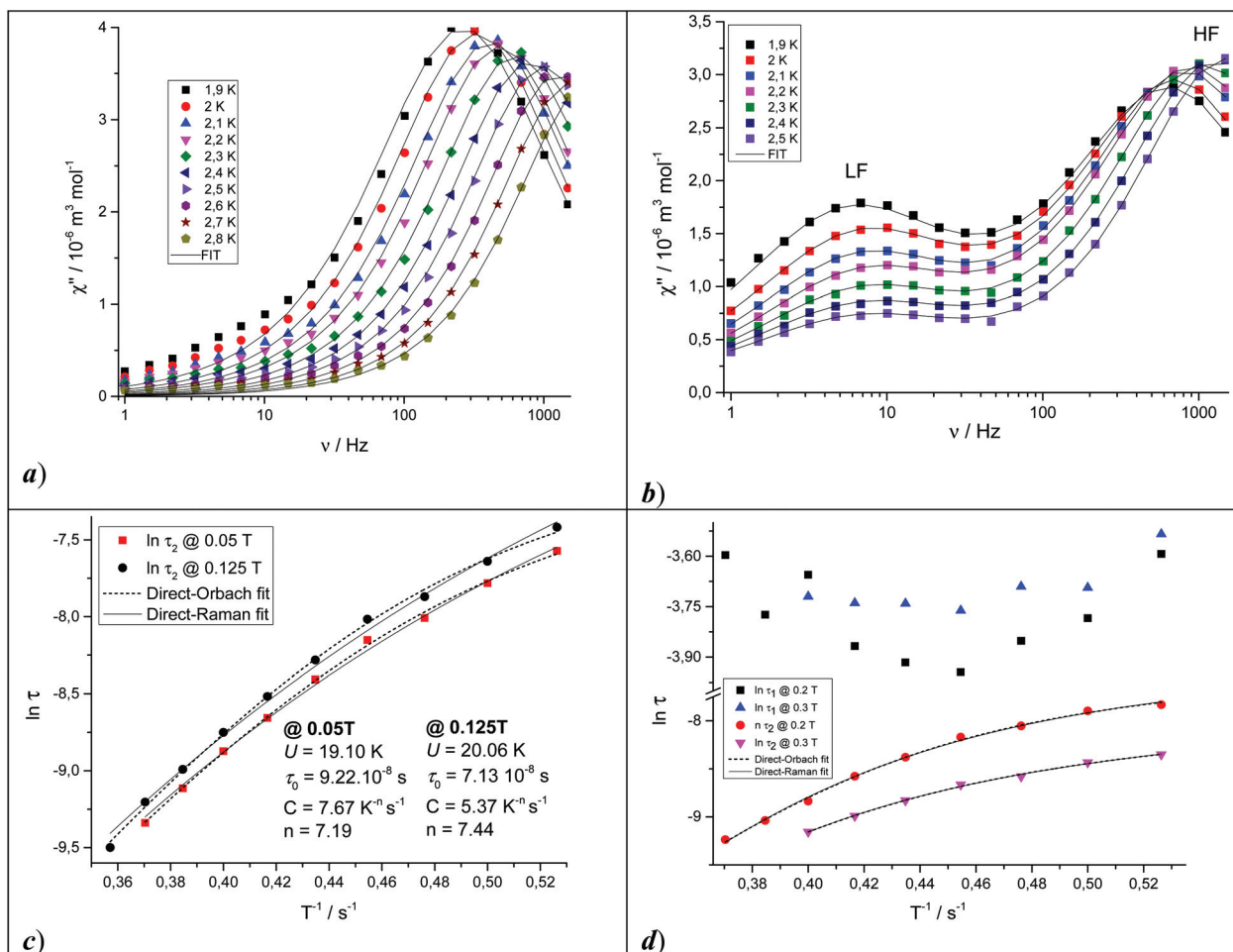


Fig. 6 Frequency dependent out-of-phase χ'' components of AC susceptibility for compound **3** recorded at an applied static magnetic field $B_{DC} = 0.125$ T (a) and $B_{DC} = 0.3$ T (b). Solid lines represent the fits using the one-component Debye model (eqn (S1) and (S2); see the ESI†) and two-component Debye model (eqn (S3) and (S4); see the ESI†), respectively. Temperature dependency of the resulting relaxation times τ_1 of the LF channel and τ_2 of the HF channel recorded at $B_{DC} = 0.05$ and 0.125 T (c); and at $B_{DC} = 0.2$ and 0.3 T. The fits of the resulting relaxation times τ_2 with the combination of the direct and Orbach processes using eqn (5) are viewed as dashed lines and the combination of the Raman and direct processes using eqn (5) are viewed as solid lines.

Orbach or single Raman term from eqn (5) helped to estimate the initial parameters for more complex fits which include combined Orbach + direct or Raman + direct terms. The best fit parameters listed in Table S4.7† are significantly different compared to those obtained at a weaker field, which is tentatively attributed to the lowered accuracy of fits caused by the co-existence of two relaxation channels. Measurements at $B_{DC} = 0.05$ T and 0.125 T resolved only the HF relaxation channel and the detailed analysis of $\tau_2(T)$ dependency allowed us to quantify the parameters of eqn (5). It is noteworthy that the values of the energy barrier and extrapolated relaxation time are highly comparable to those obtained for the isostructural chlorido complex **2** ($U = 19.1$ K, $\tau_{02} = 9.22 \times 10^{-8}$ s at 0.05 T; $U = 20.1$ K, $\tau_{02} = 9.22 \times 10^{-8}$ s at 0.125 T). The parameters of the Raman process are again lower as the expected value for a Kramers ion complex ($C = 7.7$, $n = 7.1$ at 0.05 T and $C = 5.37$, $n = 7.4$ at 0.125 T) and AB^m are again comparable with those obtained for **2** (Table S4.7, see the ESI†). AC susceptibility

investigation of **4** at $B_{DC} = 0.1$ T (Fig. 7a and Fig. S4.8, see the ESI†) revealed the presence of a single relaxation channel. Both the frequency and temperature dependence of in-phase χ' and out-of-phase χ'' components of AC susceptibility was again analysed by using the one-component Debye model which allowed us to obtain a set of relaxation times τ within the thermal range 2.0–5.2 K. Furthermore, analysis of $\tau(T)$ suggests the presence of the single Orbach or single Raman relaxation process (Fig. 7b and Table S4.8, see the ESI†). The fitted parameters of the earlier mechanism indicate the increase of the extrapolated relaxation time ($\tau_0 = 6.7 \times 10^{-7}$ s), but the decrease of the energy barrier of spin reversal ($U = 9.5$ K), when compared to pentacoordinate complexes **1–3**.

Magneto-structural correlations

Pentacoordinated high-spin Co(II) complexes with square pyramidal (SPY) and trigonal bipyramidal (TBPY) geometries are

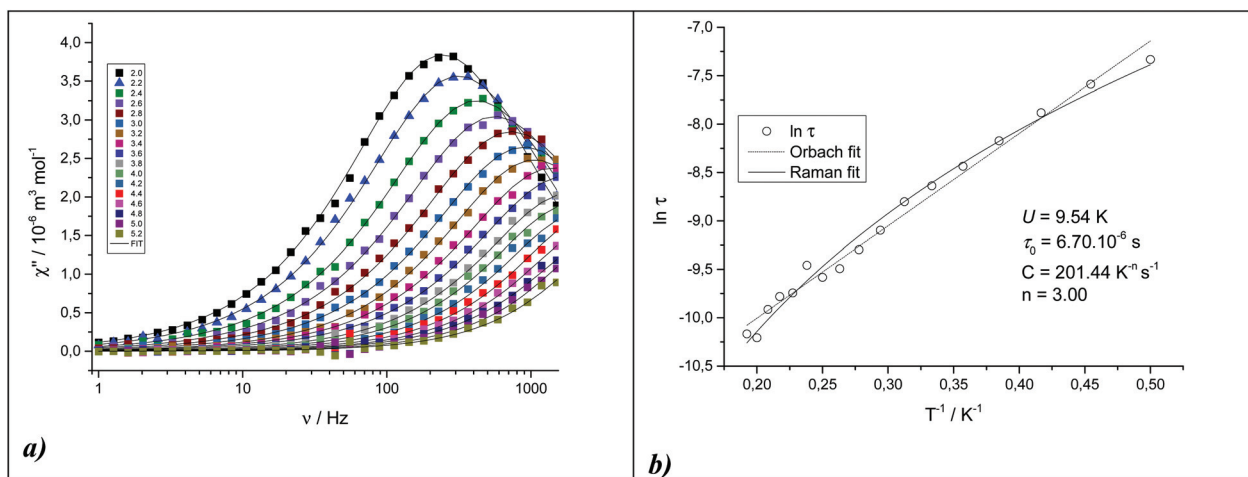


Fig. 7 Frequency dependent out-of-phase χ'' components of AC susceptibility for compound **4** recorded at the applied static magnetic field $B_{DC} = 0.1$ T (a). Solid lines represent the fits using the one-component Debye model (eqn (S1) and (S2); see the ESI†). Temperature dependency of relaxation times τ (b). The fits $\ln \tau$ vs. $1/T$ with the combination of the direct and Orbach processes using eqn (5) is viewed as dashed lines and the combination of the direct and Raman processes using eqn (5) is viewed as solid lines.

systems of great interest due to their strong magnetic anisotropy with either a negative or positive axial zero-field splitting D parameter causing the easy-axis or easy-plane type of magnetic anisotropy, respectively. The D parameters found in herein reported pentacoordinated complexes **1–3** vary in the range of 25–39 cm^{-1} , which indicates the presence of a significant interaction between the excited and ground states mediated by spin-orbit coupling. Despite the positive D values, however, the axial anisotropy can be considered due to the elevated rhombicity (Fig. 8).

As was already highlighted, the geometries of three coordination polyhedra are far from the idealised shape of SPY (**1**) or TBPY (**2** and **3**). The two isomorphous and isostructural analogues **2** and **3** show similar values of symmetry measure parameters $S(\text{TPBY})$ and τ_5 , which allows us to anticipate the comparable magnetic anisotropy. This is true only for calculated D parameters (Table 2), since the experimental D value of **2** (26 cm^{-1}) is smaller than that found for **3** (39.2 cm^{-1}) and comparable with the D parameter of **1** (24.7 cm^{-1}). The first

attempt to correlate the magnetic anisotropy with the features of coordination polyhedra involves the Addison τ_5 parameter (Fig. S5.1a, see the ESI†). The herein reported compounds **1–3** together with another 34 pentacoordinated Co(II) SIMS^{9e-n} do not indicate any trend of D with the SPY \leftrightarrow TBPY transformation suggesting that Berry pseudorotation is only one of the several contributions to the magnetic anisotropy. The shape map which involves $S(\text{SPY})$ and $S(\text{TBPY})$ symmetry measure parameters indicates that all 37 complexes show significant deviation from the ideal SPY \leftrightarrow TBPY pathway (Fig. S5.1a, see the ESI†). This correlation suggests the trend of the positive D parameters in compounds with SPY geometry often deviated towards the vacant octahedron (vOC). On the other hand, there is a group of compounds containing the tetradentate tren-type of ligand (tren = tris(2-aminoethyl)amine) with negative D and geometry close to the TBPY ($\tau_5 \approx 1$) often affected by the deformation to the Jonson trigonal bipyramid (compounds **17** [$[\text{Co}(\text{tbta})\text{N}_3](\text{ClO}_4) \cdot 3\text{MeCN}$, tbta = tris[(1-benzyl-1*H*-1,2,3-triazol-4-yl)methyl]amine),^{9j} **21** [$[\text{Co}(\text{Me}_6\text{tren})\text{Cl}]\text{ClO}_4$, $\text{Me}_6\text{tren} =$

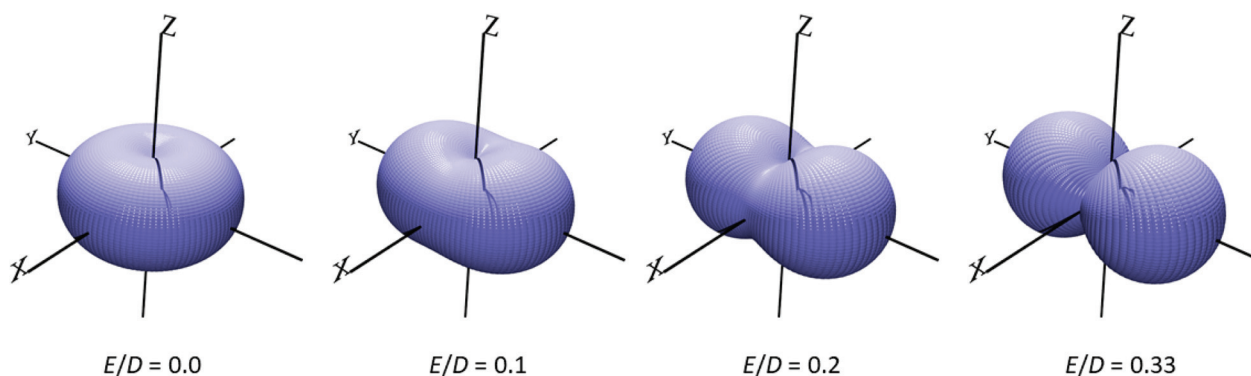
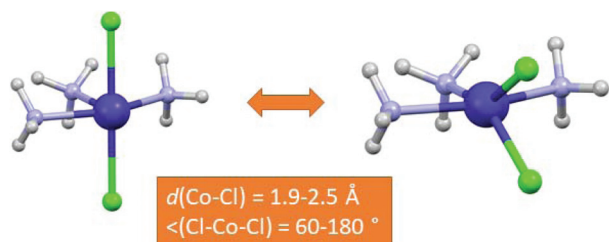


Fig. 8 The three-dimensional (3D) visualization of the molar magnetization calculated at $T = 2$ K and $B = 3$ T for $S = 3/2$ with $D = +30$ cm^{-1} and various E parameters as indicated in the plot.

tris[2-(dimethylamino)ethyl]amine),^{9k} **22** ([Co(Me₆tren)Br]Br),^{9k} **24** ([Co(NS₃^{iPr})Cl](BPh₄); NS₃^{iPr} = tris(2-(isopropylthio)ethyl)amine),^{9l} **25** ([Co(NS₃^{tBu})Cl]ClO₄; NS₃^{tBu} = tris(2-(*tert*-butylthio)ethyl)amine),^{9m} **26** ([Co(NS₃^{tBu})Br]ClO₄),^{9m} **27** ([Co(NS₃^{tBu})NCS]ClO₄),^{9m} **30** ([Co(TPMA)Cl]Cl·2.4H₂O; TPMA = tris(2-pyridylmethyl)amine),⁹ⁿ **31** ([Co(TPMA)Cl]Cl),⁹ⁿ **32** ([Co(TPMA)Br]Br·2H₂O),⁹ⁿ **33** ([Co(TPMA)Br]Br)⁹ⁿ and **34** ([Co(TPMA)I]I)⁹ⁿ.

In order to better understand the magnetic anisotropy in pentacoordinate [Co(L)X₂] systems, a simplified molecular



Scheme 2 The drawing of the model compound [Co(NH₃)₃Cl₂] and various structural parameters used for the modelling of ZFS parameters.

model was derived, in which N-donor atoms of L were replaced with ammine ligands and X was set to Cl, thus leaving us with the [Co(NH₃)₃Cl₂] model complex (Scheme 2). As the tridentate ligand L is rigid, the positions of N-atoms in [Co(NH₃)₃Cl₂] were fixed, and we focused on modelling the impact of various geometries and ligand fields induced by the variation of X ligands. Therefore, the Co–Cl bond length and Cl–Co–Cl bond angle were varied to map various shapes of the coordination polyhedron. Subsequently, CASSCF/DCD-CAS(2) calculations with CAS(7,5) were carried out to obtain ZFS parameters.

These results are then shown in the contour plot in Fig. 9. Here, the calculated *D*-values are in the range from –160 to +140 cm⁻¹ showing huge potential of this system for tuning the size of magnetic anisotropy (Fig. 9a), however, this is accompanied also by a large variation of rhombicity (Fig. 9b). In order to observe the Orbach relaxation process in SMMs, it is important to have an easy axis type of magnetic anisotropy, which can be achieved either for negative *D*-parameters or for positive *D*-parameters but with large rhombicity (*E/D* ≫ 0). Therefore, the effective *g*-factors were analysed for the first Kramers doublet for the effective spin *S*_{eff} = 1/2. If it holds that

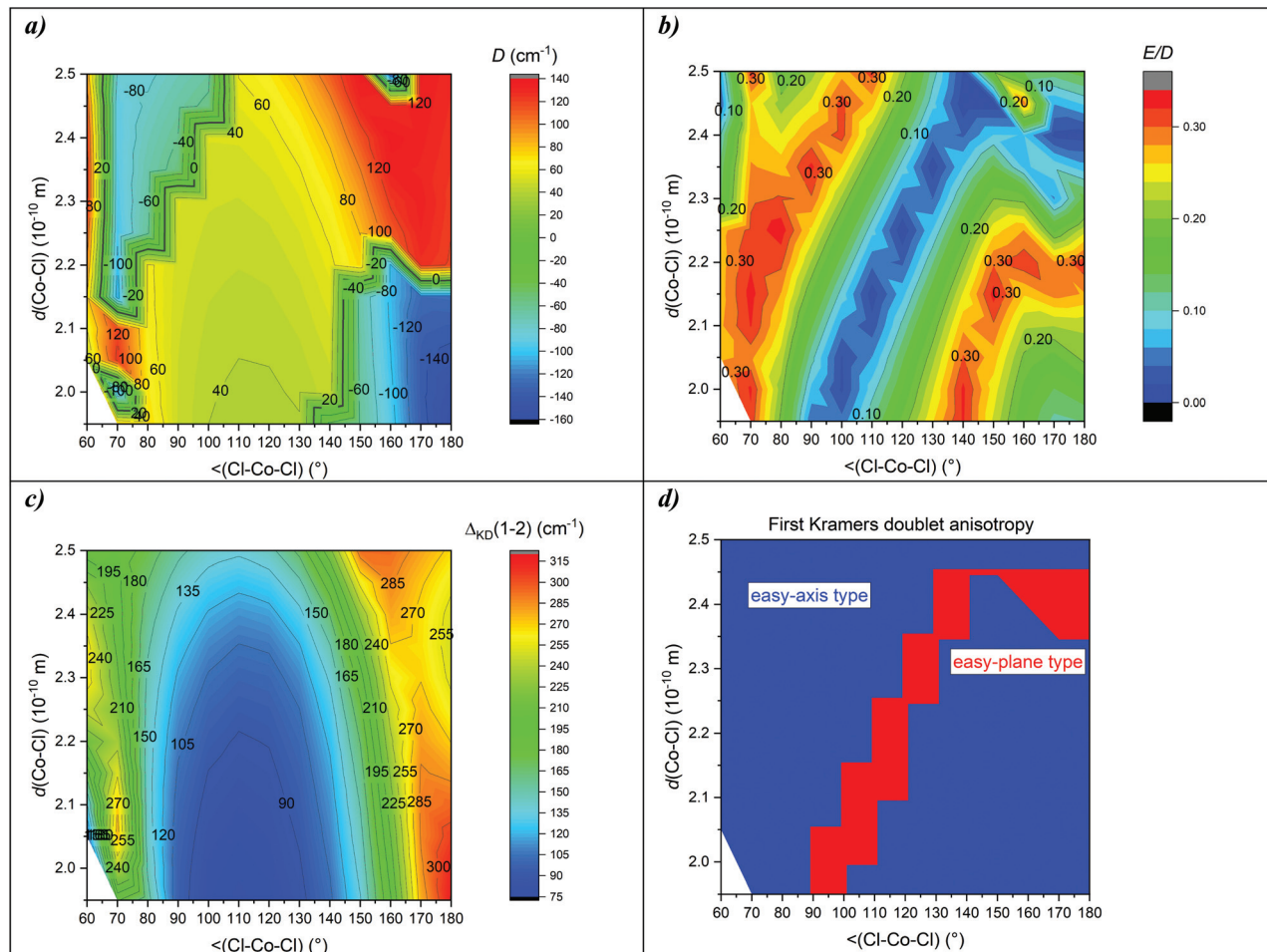


Fig. 9 The variation of ZFS parameters calculated for the [Co(NH₃)₃Cl₂] model compound using CASSCF/DCD-CAS(2) with CAS(7,5).

$g_1, g_2 < g_{\text{aver}}$ and $g_{\text{aver}} < g_3$, the easy-axis type of magnetic anisotropy of the ground state is present. In contrast, the easy-plane type of magnetic anisotropy is achieved under conditions $g_1 < g_{\text{aver}}$ and $g_{\text{aver}} < g_2, g_3$. This property is mapped in Fig. 9d, thus proving that the easy-axis type of magnetic anisotropy is achievable for a broad spectrum of tested geometries explaining also the frequent observation of the slow relaxation of the magnetization in this class of complexes. Finally, Fig. 9c shows the energy separation between the first and second Kramers doublets, which can serve to estimate maximal U_{eff} in the range $\sim 80\text{--}300\text{ cm}^{-1}$. From this point of view, the most prospective geometries are observed for either a small or large angle $\angle(\text{Cl-Co-Cl})$ (Fig. 9c), which maximizes U_{eff} .

Conclusion

In summary, we have prepared a novel tridentate ligand, the 2,6-bis(bezimidazole-1*H*-yl)pyridine derivative, containing bulky aromatic substituents in order to prevent the strong intermolecular interactions of the corresponding penta- and hexacoordinated Co(II) SIMs. The structural analysis revealed that the nature of the distortion of the coordination polyhedra in pentacoordinate complexes is notably dependent upon the nature of terminal ligand anions. While in complex **1** containing isothiocyanato terminal ligands was identified a SPY geometry with some deviation towards the shape of the vacant octahedron, the isomorphous and isostructural complexes **2** and **3** with halido Cl^- and Br^- ligands, respectively, exhibit a distorted TBPY shape of coordination polyhedra. The experimentally obtained axial zero field splitting parameters reflect the significant distortion of the coordination environments, however, their positive values along with the pronounced rhombicity obviously do not follow the trend of the distortions in $\{\text{CoN}_3\text{X}_2\}$ polyhedra. On the other hand, *ab initio* calculated D values for **2** and **3** with TBPY geometry are notably higher compared to complex **1** with the SPY shape. The ZFS spin-Hamiltonian dealing with only two lowest energy Kramers doublets is inapplicable for the description of the static magnetic properties of compound **4**. Therefore the magnetic anisotropy of the hexacoordinated Co(II) metal centre was evaluated in this case only by *ab initio* calculations, indicating the highest axial magnetic anisotropy and the lowest rhombicity within the herein reported compounds. Based on the AC susceptibility investigations, all four compounds are field induced SIMs. Two pentacoordinate complexes **1** and **2** and the ionic compound **4** show slow magnetic relaxation mediated through one high-frequency relaxation channel. However, compound **3** shows two relaxation processes, where the first low-frequency channel was pronounced only at higher DC fields and its maximum does not vary with the temperature. In contrast, the high-frequency processes found in all four compounds are very well established for SIMs based on 3d-ions and can be described by a combination of the direct one-phonon process and two-phonon Raman or Orbach processes.

Conflicts of interest

To the best of our knowledge, there are no conflicts to declare.

Acknowledgements

Grant agencies (Slovakia: APVV-18-0197, APVV-18-0016, and VEGA 1/0125/18) are acknowledged for financial support. Barbora Brachňáková acknowledges The National Scholarship Programme of the Slovak Republic for the Support of Mobility of Students, PhD Students, University Teachers and Researchers; Tatra Bank Scholarship – Students to the world 2018. Radovan Herchel and Ivan Šalitroš acknowledge the financial support from the institutional sources of the Department of Inorganic Chemistry, Palacký University Olomouc, Czech Republic. Ivan Šalitroš acknowledges the Ministry of Education, Youth and Sports of the Czech Republic under the project CEITEC 2020 (LQ1601). This article was also created with the support of the MŠVVaŠ of the Slovak Republic within the Research and Development Operational Programme for the project “University Science Park of STU Bratislava” (ITMS project no. 26240220084) co-funded by the European Regional Development Fund. We are grateful to the HPC center at the Slovak University of Technology in Bratislava, which is a part of the Slovak Infrastructure of High Performance Computing (SIVVP project, ITMS code 26230120002, funded by the European region development funds, ERDF), for the computational time and resources made available.

References

- (a) D. Gatteschi, R. Sessoli and J. Villain, *Molecular Nanomagnets*, Oxford University Press, Oxford, 2006; (b) A. Caneschi, D. Gatteschi, R. Sessoli, A. L. Barra, L. C. Brunel and M. Guillot, *J. Am. Chem. Soc.*, 1991, **113**, 5873; (c) S. Maheswaran, G. Chastanet, S. J. Teat, T. Mallah, R. Sessoli, W. Wernsdorfer and R. E. P. Winpenny, *Angew. Chem., Int. Ed.*, 2005, **44**, 5044.
- J. M. Frost, K. L. M. Harriman and M. Murugesu, *Chem. Sci.*, 2016, **7**, 2470.
- (a) R. Sessoli, D. Gatteschi, A. Caneschi and M. A. Novak, *Nature*, 1993, **365**, 141; (b) D. Gatteschi, R. Sessoli and J. Villain, *Molecular Nanomagnets*, Oxford University Press, New York, 2006; (c) Single Molecule Magnet and Related Phenomena, in *Structure and Bonding*, ed. R. E. P. Winpenny, Springer, Berlin, 2006, vol. 122; (d) J. S. Miller and D. Gatteschi, *Chem. Soc. Rev.*, 2011, **40**, 3065.
- (a) R. Boča, *Coord. Chem. Rev.*, 2004, **248**, 757; (b) O. Kahn, *Molecular Magnetism*, VCH-Verlag, Weinheim, New York, 1993.
- (a) A. K. Bar, C. Pichon and J. P. Sutter, *Coord. Chem. Rev.*, 2016, **308**, 346; (b) S. Gómez-Coca, D. Aravena, R. Morales and E. Ruiz, *Coord. Chem. Rev.*, 2015, **289**, 379.

- 6 *Lanthanides and Actinides in Molecular Magnetism*, ed. R. A. Layfield and M. Murugesu, Wiley-VCH Verlag GmbH & Co. KGaA, Weinheim, 2015.
- 7 T. Jurca, A. Farghal, P. H. Lin, I. Korobkov, M. Murugesu and D. S. Richeson, *J. Am. Chem. Soc.*, 2011, **133**, 15814.
- 8 (a) R. Mitsuhashi, S. Hosoya, T. Suzuki, Y. Sunatsuki, H. Sakiyama and M. Mikuriya, *Dalton Trans.*, 2019, **48**, 395; (b) Y. Y. Zhu, F. Liu, J. J. Liu, Y. S. Meng, S. D. Jiang, A. L. Barra, W. Wernsdorfer and S. Gao, *Inorg. Chem.*, 2017, **56**, 697; (c) S. Sottini, G. Poneti, S. Ciattini, N. Levesanos, E. Ferentinos, J. Krzystek, L. Sorace and P. Kyritsis, *Inorg. Chem.*, 2016, **55**, 9537; (d) R. Boča, J. Miklovič and J. Titiš, *Inorg. Chem.*, 2014, **53**, 2367; (e) W. Huang, T. Liu, D. Wu, J. Cheng, Z. W. Ouyang and C. Duan, *Dalton Trans.*, 2013, **42**, 15326; (f) F. Yang, Q. Zhou, Y. Zhang, G. Zeng, G. Li, Z. Shi, B. Wang and S. Feng, *Chem. Commun.*, 2013, **49**, 5289; (g) J. M. Zadrozny and J. R. Long, *J. Am. Chem. Soc.*, 2011, **133**, 20732; (h) J. M. Zadrozny, J. Telser and J. R. Long, *Polyhedron*, 2013, **64**, 209; (i) J. M. Zadrozny, J. Liu, N. A. Piro, C. J. Chang, S. Hill and J. R. Long, *Chem. Commun.*, 2012, **48**, 3927.
- 9 (a) A. K. Mondal, A. Mondal and S. Konar, *Magnetochemistry*, 2019, **5**, 12; (b) A. Switlicka, B. Machura, M. Penkala, A. Bienko, D. C. Bienko, J. Titis, C. Rajnak, R. Boca, A. Ozarowski and M. Ozerov, *Inorg. Chem.*, 2018, **57**, 12740 and references therein. (c) A. K. Mondal, J. Jover, E. Ruiz and S. Konar, *Chem. Commun.*, 2017, **53**, 5338; (d) A. K. Mondal, T. Goswami, A. Misra and S. Konar, *Inorg. Chem.*, 2017, **56**, 6870 and references therein. (e) C. Rajnák, F. Varga, J. Titiš, J. Moncol and R. Boča, *Eur. J. Inorg. Chem.*, 2017, **13**, 1915; (f) I. Nemeč, R. Herchel and Z. Trávníček, *Dalton Trans.*, 2016, **45**, 12479; (g) I. Nemeč, H. Liu, R. Herchel, X. Zhang and Z. Trávníček, *Synth. Met.*, 2016, **215**, 158; (h) I. Nemeč, R. Marx, R. Herchel, P. Neugebauer, J. van Slageren and Z. Trávníček, *Dalton Trans.*, 2015, **44**, 15014; (i) C. Rajnák, J. Titiš, O. Fuhr, M. Ruben and R. Boča, *Inorg. Chem.*, 2014, **53**, 8200; (j) D. Schweinfurth, M. G. Sommer, M. Atanasov, S. Demeshko, S. Hohloch, F. Meyer, F. Neese and B. Sarkar, *J. Am. Chem. Soc.*, 2015, **137**, 1993; (k) R. Ruamps, L. J. Batchelor, R. Guillot, G. Zakhia, A.-L. Barra, W. Wernsdorfer, N. Guihéry and T. Mallah, *Chem. Sci.*, 2014, **5**, 3418; (l) F. Shao, B. Cahier, N. Guihéry, E. Rivière, R. Guillot, A.-L. Barra, Y. Lan, W. Wernsdorfer, V. E. Campbell and T. Mallah, *Chem. Commun.*, 2015, **51**, 16475; (m) F. Shao, B. Cahier, E. Rivière, R. Guillot, N. Guihéry, V. E. Campbell and T. Mallah, *Inorg. Chem.*, 2017, **56**(3), 1104; (n) T. J. Woods, M. F. Ballesteros-Rivas, S. Gómez-Coca, E. Ruiz and K. R. Dunbar, *J. Am. Chem. Soc.*, 2016, **138**, 16407.
- 10 (a) R. Boča, C. Rajnák, J. Moncol, J. Titiš and D. Valigura, *Inorg. Chem.*, 2018, **57**, 14314; (b) L. Váhovská, S. Vitushkina, I. Potočňák, Z. Trávníček and R. Herchel, *Dalton Trans.*, 2018, **47**, 1498; (c) Y. Z. Zhang, S. Gomez-Coca, A. J. Brown, M. R. Saber, X. Zhang and K. R. Dunbar, *Chem. Sci.*, 2016, **7**, 6519; (d) R. Herchel, L. Váhovská, I. Potočňák and Z. Trávníček, *Inorg. Chem.*, 2014, **53**, 5896; (e) M. S. Fataftah, J. M. Zadrozny, D. M. Rogers and D. E. Freedman, *Inorg. Chem.*, 2014, **53**, 10716; (f) E. Colacio, K. Ruiz, E. Ruiz, E. Cremades, J. Krzystek, S. Carretta, J. Cano, T. Guidi, W. Wernsdorfer and E. K. Brechin, *Angew. Chem., Int. Ed.*, 2013, **52**, 9130.
- 11 (a) P. Antal, B. Drahoš, R. Herchel and Z. Trávníček, *Inorg. Chem.*, 2016, **55**, 5957; (b) F. Habib, I. Korobkov and M. Murugesu, *Dalton Trans.*, 2015, **44**, 6368; (c) X. C. Huang, C. Zhou, D. Shao and X. Y. Wang, *Inorg. Chem.*, 2014, **53**, 12671.
- 12 S. Alvarez and M. Llunell, *J. Chem. Soc., Dalton Trans.*, 2000, 3288.
- 13 A. W. Addison, T. Nageswara Rao, J. Reedijk, J. van Rijn and G. C. Verschoor, *J. Chem. Soc., Dalton Trans.*, 1984, 1349.
- 14 (a) F. Habib, O. R. Luca, V. Vieru, M. Shiddiq, L. Korobkov, S. I. Gorelsky, M. K. Takase, L. F. Chibotaru, S. Hill, R. H. Crabtree and M. Murugesu, *Angew. Chem., Int. Ed.*, 2013, **52**, 11290; (b) Y. Sato, Y. Nakayama and H. Yasuda, *J. Organomet. Chem.*, 2004, **689**, 744; (c) D. Gong, X. Jia, B. Wang, X. Zhang and L. Jiang, *J. Organomet. Chem.*, 2012, **702**, 10; (d) R. Cariou, J. J. Chirinos, V. C. Gibson, G. Jacobsen, A. K. Tomov, G. J. P. Britovsek and A. J. P. White, *Dalton Trans.*, 2010, **39**, 9039; (e) C. Rajnák, J. Titiš, I. Šalitroš, R. Boča, O. Fuhr and M. Ruben, *Polyhedron*, 2013, **65**, 122.
- 15 (a) S. C. Sheu, M. J. Tien, M. C. Cheng, T. Ho, S. M. Peng and Y. C. Lin, *J. Chem. Soc., Dalton Trans.*, 1995, 3503; (b) S. S. Massoud, L. Le Quan, K. Gatterer, J. H. Albering, R. C. Fischer and F. A. Mautner, *Polyhedron*, 2012, **31**, 601; (c) S. S. Massoud, F. R. Louka, R. N. David, M. J. Dartez, Q. L. Nguyn, N. J. Labry, R. C. Fischer and F. A. Mautner, *Polyhedron*, 2015, **90**, 258; (d) A. Adach, M. Daszkiewicz and B. Barszcz, *Polyhedron*, 2015, **95**, 60.
- 16 W. Addison and P. J. Burke, *J. Heterocycl. Chem.*, 1981, **18**, 803.
- 17 (a) M. Llunell, D. Casanova, J. Cirera, P. Alemany and S. Alvarez, *SHAPE version 2.0*, Universitat de Barcelona, Barcelona, Spain, 2010; (b) S. Alvarez and M. Llunell, *J. Chem. Soc., Dalton Trans.*, 2000, 3288; (c) D. Casanova, J. Cirera, M. Llunell, P. Alemany, D. Avnir and S. Alvarez, *J. Am. Chem. Soc.*, 2004, **126**, 1755; (d) S. Alvarez, D. Avnir, M. Llunell and M. Pinsky, *New J. Chem.*, 2002, **26**, 996.
- 18 (a) P. Guionneau, M. Marchivie, G. Bravic, J. F. Létard and D. Chasseau, *Top. Curr. Chem.*, 2004, **234**, 97; (b) M. A. Halcrow, *Coord. Chem. Rev.*, 2009, **253**, 2493; (c) M. A. Halcrow, *Chem. Soc. Rev.*, 2011, **40**, 4119; (d) See ESI, Fig. S2.3c† for the definition of the Σ parameter.
- 19 (a) S. Hayami, K. Murata, D. Urakami, Y. Kojima, M. Akita and K. Inoue, *Chem. Commun.*, 2008, 6510; (b) R. G. Miller, S. Narayanaswamy, J. L. Tallon and S. Brooker, *New J. Chem.*, 2014, **38**, 1932.
- 20 R. Boča, *Theoretical Foundations of Molecular Magnetism*, Elsevier, Amsterdam, 1999.
- 21 J. S. Griffith, *The theory of transition metal ions*, Cambridge University Press, London, New York, 1961.
- 22 M. E. Lines, *Phys. Rev.*, 1963, **131**, 546.
- 23 B. N. Figgis, M. Gerloch, J. Lewis, F. E. Mabbs and G. A. Webb, *J. Chem. Soc. A*, 1968, 2086–2093.

- 24 R. Boča, *A Handbook of Magnetochemical Formulae*, Elsevier, Amsterdam, 2012.
- 25 (a) F. Neese, *Wiley Interdiscip. Rev.: Comput. Mol. Sci.*, 2012, **2**, 73; (b) F. Neese, *Wiley Interdiscip. Rev.: Comput. Mol. Sci.*, 2018, **8**, e1327.
- 26 (a) C. Angeli, R. Cimiraglia and J. P. Malrieu, *Chem. Phys. Lett.*, 2001, **350**, 297; (b) C. Angeli, R. Cimiraglia, S. Evangelisti, T. Leininger and J. P. Malrieu, *J. Chem. Phys.*, 2001, **114**, 10252; (c) C. Angeli, R. Cimiraglia and J. P. Malrieu, *J. Chem. Phys.*, 2002, **117**, 9138.
- 27 (a) J. P. Perdew, K. Burke and M. Ernzerhof, *Phys. Rev. Lett.*, 1996, **77**, 3865; (b) J. P. Perdew, K. Burke and M. Ernzerhof, *Phys. Rev. Lett.*, 1997, **78**, 1396.
- 28 (a) S. Grimme, S. Ehrlich and L. Goerigk, *J. Comput. Chem.*, 2011, **32**, 1456; (b) S. Grimme, J. Antony, S. Ehrlich and H. Krieg, *J. Chem. Phys.*, 2010, **132**, 154104.
- 29 (a) M. Atanasov, D. Ganyushin, K. Sivalingam and F. Neese, in *Molecular Electronic Structures of Transition Metal Complexes II*, ed. D. M. P. Mingos, P. Day and J. P. Dahl, Springer, Berlin, Heidelberg, 2012, pp. 149–220; (b) S. K. Singh, J. Eng, M. Atanasov and F. Neese, *Coord. Chem. Rev.*, 2017, **344**, 2.
- 30 R. Maurice, R. Bastardis, C. de Graaf, N. Suaud, T. Mallah and N. Guihéry, *J. Chem. Theory Comput.*, 2009, **5**, 2977.
- 31 I. Nemeč, R. Herchel, M. Kern, P. Neugebauer, J. van Slageren and Z. Trávníček, *Materials*, 2017, **10**, 249.
- 32 (a) E. van Lenthe, E. J. Baerends and J. G. Snijders, *J. Chem. Phys.*, 1993, **99**, 4597; (b) C. van Wüllen, *J. Chem. Phys.*, 1998, **109**, 392.
- 33 (a) S. Pathak, L. Lang and F. Neese, *J. Chem. Phys.*, 2017, **147**, 234109; (b) L. Lang and F. Neese, *J. Chem. Phys.*, 2019, **150**, 104104.
- 34 R.-L. Carlin, *Magnetochemistry*, Springer-Verlag, Berlin, 1986.
- 35 (a) A. Singh and K. Shrivastava, *Phys. Status Solidi B*, 1979, **95**, 273; (b) K. N. Shrivastava, *Phys. Status Solidi B*, 1983, **117**, 437.